

Research Article

Nanobased Antibacterial Drug Discovery to Treat Skin Infections of *Staphylococcus aureus* Using *Moringa oleifera*-Assisted Zinc Oxide Nanoparticle and Molecular Simulation Study

Perumal Gobinath,¹ Ponnusamy Packialakshmi,¹ Daoud Ali,² Saud Alarifi,²
Raman Gurusamy,³ Akbar Idhayadhulla ,¹ and Radhakrishnan SurendraKumar ¹

¹PG & Research, Department of Chemistry, Nehru Memorial College (Affiliated Bharathidasan University), Puthanamapatti, Tamilnadu 621007, India

²Department of Zoology, College of Sciences, King Saud University (KSU), P.O. Box 2455, 11451 Riyadh, Saudi Arabia

³Department of Life Sciences, Yeungnam University, Gyeongsan, 38541 Gyeongsan-buk, Republic of Korea

Correspondence should be addressed to Radhakrishnan SurendraKumar; surendrakumar@nmc.ac.in

Received 16 August 2021; Revised 2 December 2021; Accepted 16 January 2022; Published 10 February 2022

Academic Editor: Aamir Jalil

Copyright © 2022 Perumal Gobinath et al. This is an open access article distributed under the Creative Commons Attribution License, which permits unrestricted use, distribution, and reproduction in any medium, provided the original work is properly cited.

In addition to the physical barrier, the epidermis acts as a natural barrier against microbial proliferation. It is prone to bacterial infections on the skin and in the nose, such as *Staphylococcus aureus*, as well as a variety of other skin illnesses. Green nanomaterial production, which eliminates the use of harmful chemicals while simultaneously reducing time, is gaining popularity in the nanotechnology area. Using the leaf extract of the pharmacologically valuable plant *Moringa oleifera*, we described a green synthesis of ZnO NPs (zinc oxide nanoparticles). ZnO NPs had a particle size of 201.6 nm and a zeta potential of -56.80 mV, respectively. A novel aminoketone antibacterial medication was synthesized and tested for antibacterial activity using ZnO NPs as a photocatalyst in this work. This method produces high yields while maintaining efficient and gentle reaction conditions. *Moringa oleifera* extract can reduce ZnO to ZnO NPs in a straightforward manner. FT-IR, ¹H-NMR, ¹³C-NMR, mass spectra, elemental analysis, and morphological analysis were used to synthesize and describe the antibacterial medicines (1a-1g) and (2a-2g). In addition, antibacterial activity was evaluated against bacteria such as *Enterococcus faecalis* and *Staphylococcus aureus*, and compound 1c (63 µg/mL, *E. faecalis*) and compound 2e (0.12 µg/mL, *S. aureus*) were found to be very active when compared to other medications. mupirocin is used as a reference. In addition, studies of in silico molecular docking for the bacterial DsbA protein were conducted. The strong molecules 1c (-4.3 kcal/mol) and 2e (-5.1 kcal/mol) exhibit a high binding affinity through hydrogen bonding, according to docking tests.

1. Introduction

The skin is the first line of protection against germs and bacteria among the body's primary organs. The integrity of the skin is jeopardized when it is damaged. Despite substantial research into wound healing mechanisms, many topics remain unresolved. Because of its physical, chemical, and microbiological qualities, the skin is a crucial barrier in wound closure. The physiological regulation of skin wound

healing is more complicated than you may expect since many distinct cell types and mediators interact in a complex way [1]. The transition between the inflammatory and proliferative stages of wound repair is currently the subject of a lot of research [2]. To begin, skin cells are exposed to acute phase signals such as damage-associated or pathogen-specific molecular patterns, which are identified on their parts by toll-like receptors, causing inflammation to begin and continue [3, 4]. Figure 1 depicts a multilayered skin. A decreased

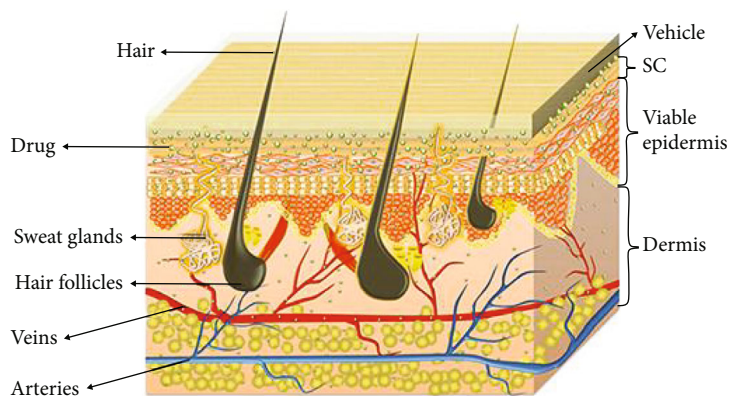


FIGURE 1: Multilayer of skin [5].

capillary count may be enough to promote normal skin regeneration as long as nutritional perfusion is provided. *Staphylococcus aureus* is a common cutaneous bacteria that can be found on the skin, in nasal cavities, and in the respiratory tract. Figure 2 illustrates skin injury caused by *Staphylococcus aureus*.

Antibacterial nanoparticles can operate as a transporter for antibiotics, boosting their bioavailability and efficiency [6]. Antibacterial nanoparticles are made from a variety of materials, including metals, and do not require the usage of pharmaceuticals. Antibiotic delivery for bacterial killing is improved by lowering side effects and drug resistance through nonmedical techniques. Nanoparticles are made from a number of materials and can be utilized for a variety of purposes. Many types of nanoformulations are used for antibacterial applications. The nanoparticle core or layer can contain numerous drugs for drug delivery. Metallic nanoparticles, primarily comprised of Zn, Au, Ag, or Cu, have been discovered to have potent antibacterial properties [7].

Antibacterial medicine has grown in popularity because to its low cost, environmental friendliness, potential for synthesis in ambient air, and lack of toxicity. Green synthesis has recently become the favored method for nanoparticle synthesis [8]. Furthermore, key ZnO NP applications in environmental and biological sectors such as drug administration, biological sensing, biological labeling, gene transfer, and nanomedicine have been reported [9–16]. Antibacterial, antidiabetic, antifungal, acaricidal, predelicidal, and larvicidal properties of ZnO NPs have also been reported [17–21].

Nitrogen-containing compounds are key components present in a diverse range of physiologically active substances. A range of biologically significant chemicals contains nitrogen, which is found in amino ketone compounds. Natural and synthetic herbicides and medications that inhibit 4-hydroxyphenylpyruvate dioxygenase have the cyclohexane-1,3-dione skeleton [22–24].

The Mannich reaction has been widely used as one of the promising multicomponent reactions (MCRs) in the recent decade due to its performance in the creation of carbon–nitrogen (C–N) and carbon–carbon (C–C) single bonds. Synthetic chemists and the pharmaceutical industry have been paying special attention to the asymmetric Mannich reaction, which



FIGURE 2: *Staphylococcus aureus* affected skin.

is a useful transformation for accessing amine-containing building blocks [25]. As a result, numerous uses of Mannich bases as potential biological agents have been documented. The starting ingredients for the manufacture of triketone herbicides, which function as inhibitors of the transformation route in plants and animals, are 1,3-cyclohexanedione and its derivatives. 2-cyclohexanedione, one of these herbicides, is so selective and effective that it causes tyrosinemia [26] shown in Figure 3.

Based on the above report to combat antibiotic resistance, researchers are seeking new approaches to enhance the therapeutic efficacy of existing antibiotics and develop new antibiotics of 1,3-cyclohexanedione derivatives that are prepared by using the nanoparticle catalyst. The synthesis of 1,3-cyclohexanedione derivatives showed an affordable, reusable catalyst, and enhanced reaction conditions. We are attempting to use ZnO NPs as a green catalyst for the production of 1,3-cyclohexanedione derivatives in this study. We provide a straightforward approach for synthesizing and analyzing ZnO NPs, which were used as a potent and effective green catalyst in the production of substituted 1,3-cyclohexanedione, substituted aldehydes, and urea/thiourea. FT-IR, NMR ($^1\text{H-NMR}$ & $^{13}\text{C-NMR}$), mass, elemental analysis, XRD, SEM, and TEM were used to determine the structure and morphology of the newly synthesized antibacterial medicines, which were then tested for antibacterial activity.

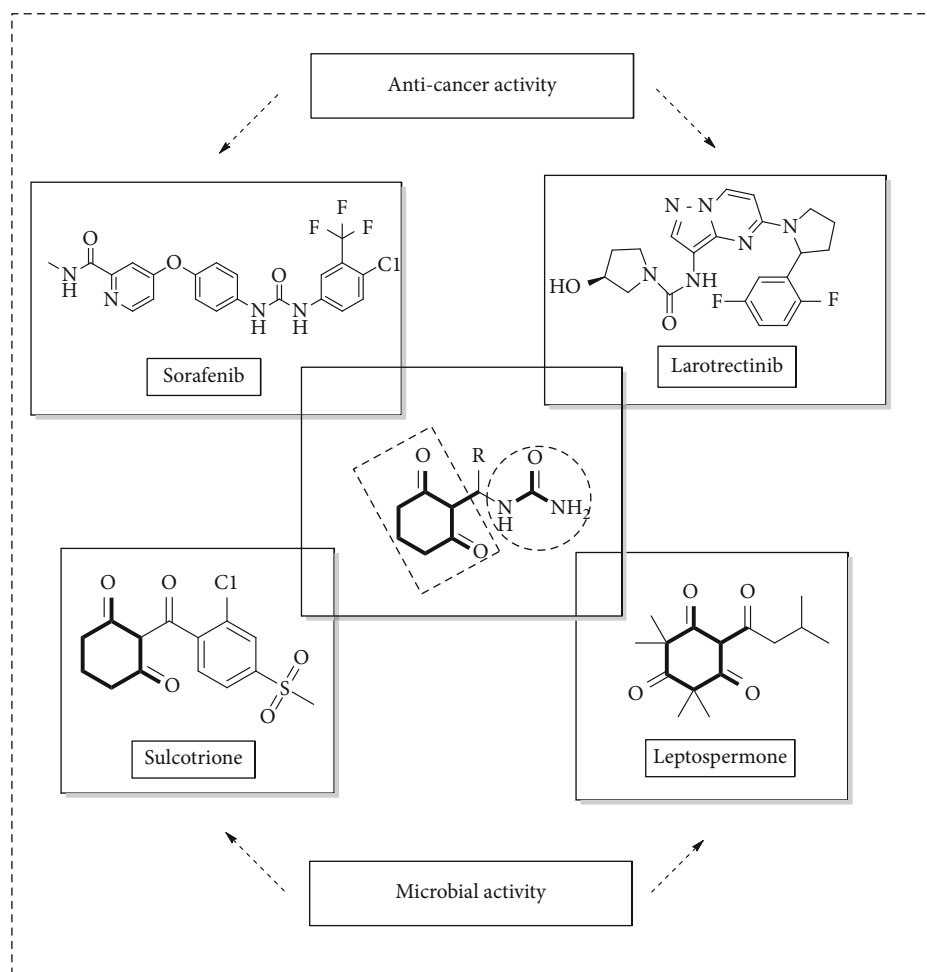


FIGURE 3: Antibacterial and anticancer active urea and 1,3-cyclohexanedione agents.

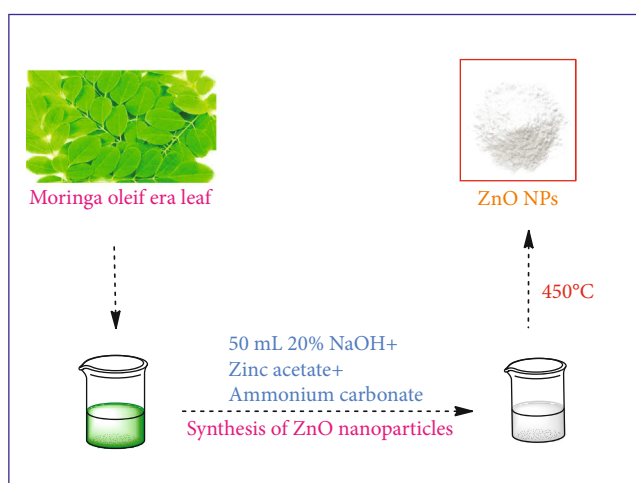


FIGURE 4: Synthesis of ZnO NPs from *Moringa oleifera*.

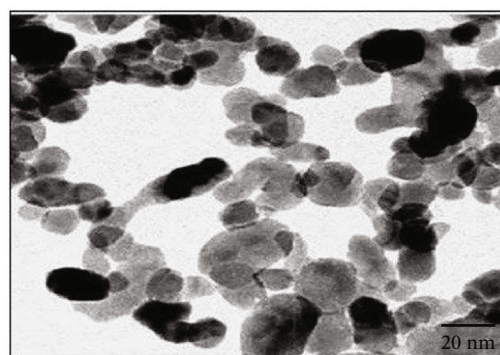


FIGURE 5: TEM image of ZnO nanoparticles.

2. Materials and Methods

All the chemicals, such as 1,3-cyclohexanedione, substituted aldehydes, urea, and thiourea, were attained from Sigma-Aldrich. Melting points have been observed in open capillary

tubes. The IR spectrum measurements were performed in KBr on a Shimadzu 8201pc ($4000\text{--}400\text{ cm}^{-1}$). The ^1H and ^{13}C NMR spectra were performed on a Bruker DRX-300 MHz. In order to analyze the elements (C, H, and N), an elemental analyzer (Varian EL III) was used. SEM, XRD, and TEM are used to verify the morphology of ZnO NPs by using a Benchtop PROTO AXRD, and XRD patterns that were measured by using $\text{CuK}\alpha$ targets and Ni-filters between 10 and 80 nm. We investigated SEM research by



FIGURE 6: SEM image of ZnO nanoparticles.

using a scanning electron microscope (SEM) model VP-1450 (LEO, Co., Germany). An instrument LEO 912 AB was used to analyze the sample by transmission electron microscopy (TEM). A TLC analysis was performed to determine purity (using hexane as an eluting solvent) and separated by column chromatography.

A substituted benzaldehyde (1.0 mL, 0.01 mol), primary amine (urea) (0.60 g, 0.01 mol), and 1,3-cyclohexanedione (1.12 g, 0.01 mol) were refluxed for 2 hrs using ethanol as a solvent with using ZnO NP catalyst. The obtained solid 1-((2,6-dioxocyclohexyl)(phenyl) methyl) urea 1a was allowed to cool and then poured into ice water. The purity of the compound was checked by thin layer chromatography (TLC). The precipitate was recrystallized with ethanol. A similar procedure was carried out with the remaining synthesized compounds (1b-2g).

2.1. Preparation of *Moringa oleifera* Leaf Extract. 5 grams of *Moringa oleifera* leaves was washed completely with distilled water, and both surfaces of leaves were sterilized using alcohol by delicate scouring. These leaves were warmed for 45 min in 100 mL of distilled water at 60°C. Then, the extract was filtered with Whatman 41 filter paper. The filtrate was put away in a cool and dry spot.

2.1.1. Synthesis of ZnO NPs. For the synthesis of ZnO NPs by precipitation reaction process, 20 mL of *Moringa oleifera* leaf extract was blended in with 60 mL 20% NaOH solution. Then, at that point, 5 mL arrangements of that combination and 60 mL refined water were taken in a 250 mL measuring glass and continued blending for 1.5 h. Then, zinc acetate (2.1 g in 100 mL water) and ammonium carbonate (0.95 g in 100 mL) solutions were added drop insightful into the measuring glass all the while with steady mixing. After finish of the reaction, the suspension was continued mixing at

750 rpm for 1 h at 30°C temperature. At long last, precipitate was filtered and washed with ammonia solution followed by ethanol for several times. Then, the precipitates were dried under vacuum for 13 hours and calcinated in a hot air oven at 350°C for 4.5 hours shown in Figure 4. The presence of white powder is an obvious sign of the development of ZnO NPs framed in the response combination. Then, at that point, ZnO NPs were gathered and put away in vacuum for additional utilization [27].

Synthesis of 1-((2,6-dioxocyclohexyl)(phenyl)methyl) urea (1a): yield: 87%. White solid; M.p: 172°C; IR (KBr, cm^{-1}). 3445 (NH_2 -Str), 2960 (NH), and 1717 (C=O); ^1H NMR (300 MHz, CDCl_3) δ 8.21 (s, 1H, NH), 7.41-7.28 (Ph, m, 5H), 5.50 (d, $J = 1.7$ Hz, 1H, Ph-CH), 5.47 (s, 2H, NH_2), 4.24 (d, $J = 6.9$ Hz, 1H, CHD), and 2.44-1.99 (m, 6H, CHD); ^{13}C NMR (300 MHz, CDCl_3) δ 203.82, 167.60, 142.18, 133.64, 128.77, 127.02, 126.25, 76.57, 62.01, 39.64, and 18.77; EI-MS (relative intensity %): m/z 261.12 (M^+ , 15%); elemental analysis: anal. ($\text{C}_{14}\text{H}_{16}\text{N}_2\text{O}_3$): C, 64.62; H, 6.22; and N, 10.79. Found: C, 64.64; H, 6.25; and N, 10.81.

Synthesis of 1-((2,6-dioxocyclohexyl)(3-nitrophenyl)-methyl) urea (1b) is as follows: yield: 89%; yellow solid; M.p: 164°C; IR (KBr, cm^{-1}). 3405 (NH_2 -Str), 3025 (NH), 1710 (C=O), and 1530 (NO_2); ^1H NMR (300 MHz, CDCl_3) δ 8.25 (s, 1H, NH), 8.24-7.78 (m, 4H, Ph- NO_2), 5.56 (s, 2H, NH_2), 5.51 (d, $J = 1.6$ Hz, 1H, CH-Ph), 4.21 (d, $J = 8.0$ Hz, 1H, CHD), and 2.30-1.97 (m, 6H, CHD); ^{13}C NMR (300 MHz, CDCl_3) δ 203.87, 167.62, 150.03, 142.18, 133.94, 128.77, 124.38, 120.36, 77.00, 58.83, 39.09, and 18.77; EI-MS (relative intensity %): m/z 306.10 (M^+ , 16%); elemental analysis: anal. ($\text{C}_{14}\text{H}_{15}\text{N}_3\text{O}_5$): C, 55.09; H, 4.96; and N, 13.79. Found: C, 55.07; H, 4.94; and N, 13.76.

Synthesis of 1-((4-chlorophenyl)(2,6-dioxocyclohexyl)-methyl) urea (1c) is as follows: yield: 94%; sandle solid; M.p: 190°C; IR (KBr, cm^{-1}). 3485 (NH_2 -Str), 2947 (NH), 1723

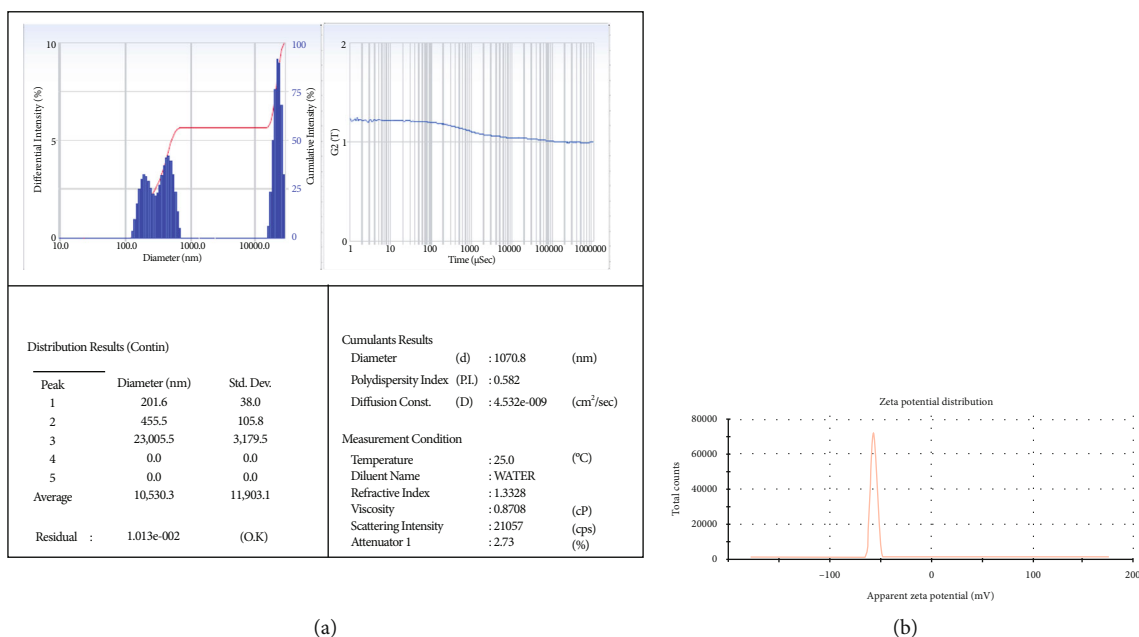


FIGURE 7: Particle size distributions and zeta potential peak of ZnO NPs.

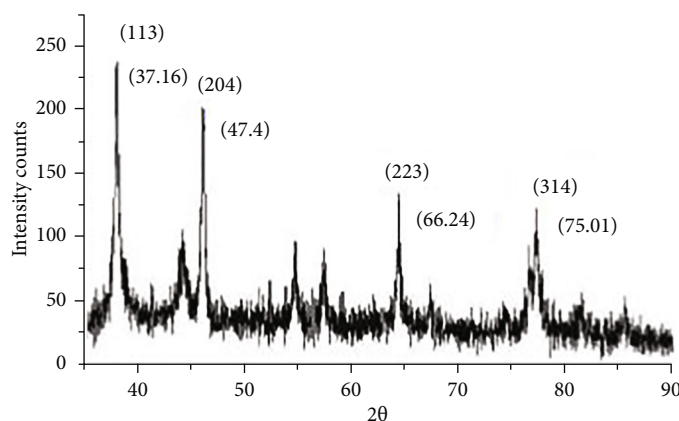


FIGURE 8: XRD patterns of ZnO nanoparticles.

(C=O), and 837 (Cl); ¹H NMR (300 MHz, CDCl₃), δ 8.25 (s, 1H, NH), 7.46-7.35 (m, 4H, Ph-Cl), 5.58 (s, 2H, NH₂), 5.52 (d, *J* = 1.5 Hz, 1H, CH-Ph), 4.26 (d, *J* = 6.5 Hz, 1H, CHD), and 2.63-1.95 (m, 6H, CHD); ¹³C NMR (300 MHz, CDCl₃) δ 203.85, 167.64, 142.84, 133.64, 128.67, 127.62, 77.43, 62.01, 39.37, and 18.84; EI-MS (relative intensity %): *m/z* 296.07 (M⁺,16); elemental analysis: anal. (C₁₄H₁₅ClN₂O₃): C, 57.04; H, 5.15; and N, 9.51. Found: C, 57.06; H, 5.14; and N, 9.50.

Synthesis of 1-((2,6-dioxocyclohexyl)(4-hydroxyphenylmethyl) urea (1d) is as follows: yield: 92%; light yellow solid; M.p: 148°C; IR (KBr, cm⁻¹). 3412 (NH₂-Str), 2908 (NH), 1752 (C=O), and 1465 (OH); ¹H NMR (300 MHz, CDCl₃) δ 8.08 (s, 1H, NH), 7.41-6.73 (m, 4H, Ph-OH), 5.55 (s, 2H, NH₂), 5.43 (d, *J* = 1.7 Hz, 1H, CH-Ph), 5.30 (s, 1H, OH), 4.28 (d, *J* = 6.9 Hz, 1H, CHD), and 2.41-1.99 (m, 6H, CHD); ¹³C

NMR (300 MHz, CDCl₃) δ 203.83, 167.62, 157.54, 136.18, 127.02, 115.50, 77.00, 62.01, 39.37, and 18.77; EI-MS (relative intensity %): *m/z* 277.11 (M⁺,15); elemental analysis: anal. (C₁₄H₁₆N₂O₄): C, 60.85; H, 5.85; and N, 10.15. Found: C, 60.86; H, 5.86; and N, 10.17.

Synthesis of 1-((2,6-dioxocyclohexyl)(4-hydroxy-methoxyphenyl)methyl) urea (1e) is as follows: yield: 95%; white solid; M.p: 184°C; IR (KBr, cm⁻¹). 3465 (NH₂-Str), 3152 (NH), 1701 (C=O), 1402 (OCH₃), and 3387 (OH); ¹H NMR (300 MHz, CDCl₃) δ 8.26 (s, 1H, NH), 7.41-7.38 (m, 5H, Ph), 5.54 (s, 2H, NH₂), 5.52 (d, *J* = 1.9 Hz, 1H, CH-Ph), 5.38 (s, 1H, OH), 4.24 (d, *J* = 6.9 Hz, 1H, CHD), 3.85 (s, 3H, OCH₃), and 2.43-1.97 (m, 6H, CHD); ¹³C NMR (300 MHz, CDCl₃) δ 203.87, 167.67, 146.25, 131.94, 122.01, 120.36, 115.50, 109.46, 77.43, 62.01, 54.38, 39.09, and 18.84; EI-MS (relative

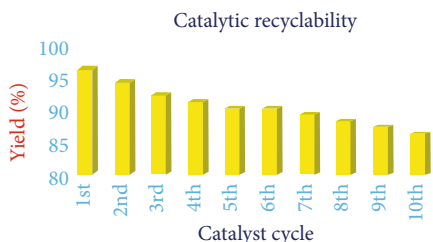


FIGURE 9: Recyclability of ZnO NPs.

TABLE 1: Catalyst recyclability.

Entry	Catalyst use	Yield (%)
1	1 st	96
2	2 nd	94
3	3 rd	92
4	4 th	91
5	5 th	90
6	6 th	90
7	7 th	89
8	8 th	88
9	9 th	87
10	10 th	86

TABLE 2: Substitution of synthesized compounds 1a-1g and 2a-2g.

Compounds	R	X
1a	Ph-CHO	O
1b	3-NO ₂ -Ph-CHO	O
1c	4-Cl-Ph-CHO	O
1d	4-OH-Ph-CHO	O
1e	4-OH-3-OCH ₃ -Ph-CHO	O
1f	2-OH-Ph-CHO	O
1g	4-OCH ₃ -Ph-CHO	O
2a	Ph-CHO	S
2b	3-NO ₂ -Ph-CHO	S
2c	4-Cl-Ph-CHO	S
2d	4-OH-Ph-CHO	S
2e	4-OH-3-OCH ₃ -Ph-CHO	S
2f	2-OH-Ph-CHO	S
2g	4-OCH ₃ -Ph-CHO	S

intensity %): m/z 307.12 (M⁺,17%); elemental analysis: anal. (C₁₅H₁₈N₂O₅): C, 58.80; H, 5.90; and N, 26.11. Found: C, 58.82; H, 5.92; and N, 26.12.

Synthesis of 1-((2,6-dioxocyclohexyl)(2-hydroxyphenyl)methyl) urea (1f) is as follows: yield: 85%; white solid; M.p: 204°C; IR (KBr, cm⁻¹). 3475 (NH₂-Str), 3412 (OH), 2934 (NH), and 1760 (C=O); ¹H NMR (300 MHz, CDCl₃) δ 8.72 (s, 1H, NH), 7.35-6.73 (m, 4H, Ph), 5.74 (s, 2H, NH₂), 5.54 (d, J = 2.5 Hz, 1H, CH-Ph), 5.33 (s, 1H, OH),

4.33 (d, J = 6.9 Hz, 1H, CHD), and 2.49-1.95 (m, 6H, CHD); ¹³C NMR (300 MHz, CDCl₃) δ 203.99, 167.62, 156.54, 131.73, 128.77, 127.02, 121.94, 115.50, 77.43, 62.01, 39.37, and 18.77; EI-MS (relative intensity %): m/z 277.11 (M⁺,15); elemental analysis: anal. (C₁₄H₁₆N₂O₄): C, 60.88; H, 5.85; and N, 10.15. Found: C, 60.86; H, 5.86; and N, 10.17.

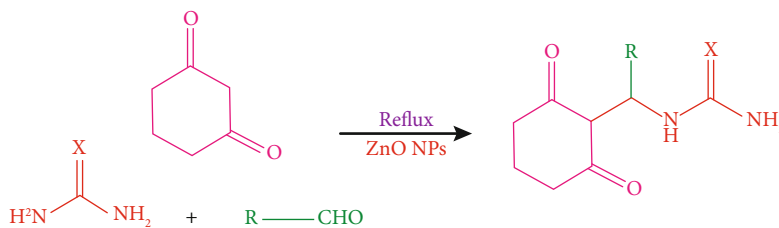
Synthesis of 1-((2,6-dioxocyclohexyl)(4-methoxyphenyl)methyl) urea (1g) is as follows: yield: 88%; sandle solid; M.p: 244°C; IR (KBr, cm⁻¹). 3455 (NH₂-Str), 2925 (NH),1740 (C=O), and 1402 (OCH₃); ¹H NMR (300 MHz, CDCl₃) δ 8.38 (s, 1H, NH),6.92-6.69 (m, 4H, Ph), 5.68 (s, 2H, NH₂), 5.51 (d, J = 1.3 Hz,1H, CH-Ph), 4.38 (d, J = 7.2 Hz, 1H, CHD), 3.89 (s, 3H, OCH₃), and 2.55-1.93 (m, 6H, CHD); ¹³C NMR (300 MHz, CDCl₃) δ 203.99, 168.01, 158.60, 135.81, 126.61, 114.10, 76.69, 62.30, 55.80, 39.75, and 18.84; EI-MS (relative intensity%): m/z 291.13 (M⁺,16%); elemental analysis: anal. (C₁₅H₁₈N₂O₄): C, 62.08; H, 6.28; and N, 9.68. Found: C, 62.06; H, 6.26; and N, 9.66.

Synthesis of 1-((2,6-dioxocyclohexyl)(phenyl)methyl) thiourea (2a) is as follows: yield: 86%; white solid; M.p: 232°C; IR (KBr, cm⁻¹).3420 (NH₂-Str), 2975 (NH), and 1701 (C=O); ¹H NMR (300 MHz, CDCl₃) δ 8.31 (s, 1H, NH), 7.42-7.38 (m, 5H, Ph), 5.61 (s, 2H, NH₂), 5.43 (d, J = 1.5 Hz, 1H, CH-Ph), 4.31 (d, J = 6.9 Hz, 1H, CHD), and 2.44-1.85 (m, 6H, CHD); ¹³C NMR (300 MHz, CDCl₃) δ 203.94, 182.01,142.18, 133.48, 128.77, 127.04, 126.78, 76.57, 62.25, 39.68, and 18.79; EI-MS (relative intensity %): m/z 277.10 (M⁺,15%); elemental analysis: anal. (C₁₄H₁₆N₂O₂S): C, 64.62; H, 6.22; and N, 10.78. Found: C, 64.64; H, 6.24; and N, 10.76.

Synthesis of 1-((2,6-dioxocyclohexyl)(3-nitrophenyl)methyl) thiourea (2b) is as follows: yield: 84%; white solid; M.p: 264°C; IR (KBr, cm⁻¹). 3490 (NH₂-Str), 2960 (NH), 1723 (C=O), and 1510 (NO₂); ¹H NMR (300 MHz, CDCl₃) δ 8.32 (s, 1H, NH), 8.24-7.78 (m, 4H, Ph-NO₂), 5.62 (s, 2H, NH₂), 5.44 (d, J = 1.5 Hz, 1H, CH-Ph), 4.32 (d, J = 6.9 Hz, 1H, CHD), and 2.45-1.88 (m, 6H, CHD); ¹³C NMR (300 MHz, CDCl₃) δ 203.95, 182.02, 150.10, 142.60, 133.94, 129.23, 124.88, 120.77, 76.62, 62.26, 39.64, and 18.80; EI-MS (relative intensity %): m/z 322.08 (M⁺,17%); elemental analysis: anal. (C₁₄H₁₅N₃O₄S): C, 55.02; H, 4.91; and N, 13.72. Found: C, 55.04; H, 4.93; and N, 13.74.

Synthesis of 1-((4-chlorophenyl)(2,6-dioxocyclohexyl)methyl) thiourea (2c) is as follows: yield: 75%; white color solid; M.p: 202°C; IR (KBr, cm⁻¹). 3424 (NH₂-Str), 2925 (NH), 1745 (C=O), and 748 (Cl); ¹H NMR (300 MHz, CDCl₃) δ 8.33 (s, 1H, NH), 7.46-7.28 (m, 4H, Ph-Cl), 5.63 (s, 2H, NH₂), 5.45 (d, J = 1.5 Hz, 1H, CH-Ph), 4.33 (d, J = 6.9 Hz, 1H, CHD), and 2.46-1.80 (m, 6H, CHD); ¹³C NMR (300 MHz, CDCl₃) δ 203.96, 182.03, 141.70, 133.47, 128.69, 127.64, 76.63, 62.27, 39.70, and 18.81; EI-MS (relative intensity %): m/z 312.05 (M⁺,15%); elemental analysis: anal. (C₁₄H₁₅ClN₂O₂S): C, 57.12; H, 5.18; and N, 9.52. Found: C, 57.14; H, 5.16; and N, 9.54.

Synthesis of 1-((2,6-dioxocyclohexyl)(4-hydroxyphenyl)methyl) thiourea (2d) is as follows: yield: 83%; white color solid; M.p: 240°C; IR (KBr, cm⁻¹). 3425 (NH₂-Str), 2948 (NH), 1770 (C=O), and 1445 (OH); ¹H NMR (300 MHz, CDCl₃) δ 8.34 (s, 1H, NH), 7.14-6.78 (m, 4H, Ph-OH), 5.64 (s, 2H, NH₂), 5.46 (d, J = 1.5 Hz, 1H, CH-Ph), 4.34 (d,

SCHEME 1: Synthesis of β -aminoketone derivatives.

$J = 6.9$ Hz, 1H, CHD), 5.30 (s, 1H, OH), and 2.47-1.85 (m, 6H, CHD); ^{13}C NMR (300 MHz, CDCl_3) δ 203.97, 182.04, 156.52, 136.15, 127.04, 115.73, 76.64, 62.28, 39.71, and 18.82; EI-MS (relative intensity %): m/z 293.09 (M^+ , 17%); elemental analysis: anal. ($\text{C}_{14}\text{H}_{16}\text{N}_2\text{O}_3\text{S}$): C, 60.80; H, 5.85; and N, 10.15. Found: C, 60.82; H, 5.83; and N, 10.17.

Synthesis of 1-((2,6-dioxocyclohexyl)(4-hydroxy-3-methoxyphenyl)methyl) thiourea (2e) is as follows: yield: 85%; white color solid; M.p: 254°C ; IR (KBr, cm^{-1}). 3465 (NH_2 -Str), 3410 (OH), 3130 (NH), 1644 ($\text{C}=\text{O}$), and 1424 ($-\text{OCH}_3$); ^1H NMR (300 MHz, CDCl_3) δ 8.57 (s, 1H, NH), 7.04-6.42 (m, 5H, Ph), 5.52 (s, 2H, NH_2), 5.36 (s, 1H, OH), 4.35 (d, $J = 1.5$ Hz, 1H, CH-Ph), 3.80 (s, 3H, OCH_3), 2.64 (d, $J = 6.9$ Hz, 1H, CHD), and 2.43-1.62 (m, 6H, CHD); ^{13}C NMR (300 MHz, CDCl_3) δ 203.98, 182.05, 146.64, 132.82, 122.46, 121.20, 115.61, 110.10, 76.65, 62.29, 39.73, and 18.86; EI-MS (relative intensity %): m/z 323.10 (M^+ , 17%); elemental analysis: anal. ($\text{C}_{15}\text{H}_{18}\text{N}_2\text{O}_4\text{S}$): C, 55.82; H, 5.60; and N, 8.62. Found: C, 55.85; H, 5.62; and N, 8.64.

Synthesis of 1-((2,6-dioxocyclohexyl)(2hydroxyphenyl)methyl) thiourea (2f) is as follows: yield: 81%; white color solid; M.p: 276°C ; IR (KBr, cm^{-1}). 3495 (NH_2 -Str), 3415 (OH), 2945 (NH), and 1762 ($\text{C}=\text{O}$); ^1H NMR (300 MHz, CDCl_3) δ 8.68 (s, 1H, NH), 7.16-6.92 (m, 4H, Ph), 5.65 (s, 2H, NH_2), 5.49 (d, $J = 1.5$ Hz, 1H, CH-Ph), 5.37 (s, 1H, OH), 4.37 (d, 1H, CHD), and 2.50-1.88 (m, 6H, CHD); ^{13}C NMR (300 MHz, CDCl_3) δ 204.00, 182.06, 154.60, 130.95, 128.46, 126.60, 121.15, 115.74, 76.66, 62.37, 39.76, and 18.85; EI-MS (relative intensity %): m/z 293.09 (M^+ , 17%); elemental analysis: anal. ($\text{C}_{14}\text{H}_{16}\text{N}_2\text{O}_3\text{S}$): C, 57.53; H, 5.53; and N, 9.57. Found: C, 57.55; H, 5.55; and N, 9.59.

Synthesis of 1-((2,6-dioxocyclohexyl)(4-methoxyphenyl)methyl) thio urea (2g) is as follows: yield: 92%; white color solid; M.p: 298°C ; IR (KBr, cm^{-1}). 3460 (NH_2 -Str), 2930 (NH), 1744 ($\text{C}=\text{O}$), and 1434 (OCH_3); ^1H NMR (300 MHz, CDCl_3) δ 8.39 (s, 1H, NH), 6.93-6.72 (m, 4H, Ph), 5.66 (s, 2H, NH_2), 5.50 (d, $J = 1.5$ Hz, 1H, CH-Ph), 4.37 (d, $J = 6.9$ Hz, 1H, CHD), 4.37 (d, 1H, CHD), 3.85 (s, 3H, OCH_3), and 2.51-1.89 (m, 6H, CHD); ^{13}C NMR (300 MHz, CDCl_3) δ 204.02, 182.07, 159.62, 135.82, 126.64, 115.12, 76.67, 62.32, 55.90, 39.77, and 18.86; EI-MS (relative intensity %): m/z 307.11 (M^+ , 16%); elemental analysis: anal. ($\text{C}_{15}\text{H}_{18}\text{N}_2\text{O}_3\text{S}$): C, 58.42; H, 5.93; N, 9.15. Found: C, 58.44; H, 5.94; and N, 9.17.

2.2. Molecular Docking Study. A computational in silico study, including molecular docking simulation, was evaluated using the Red Hat 5.1 Linux platform running on a Lenovo PC with

an Intel core I7-6700 processor from Schrodinger Maestro 9.2 version, LLC, NY. In this study, a (PDB ID: 4WET, DOI: 10.2210/pdb4WET/pdb) file for target proteins was downloaded from the Protein Data Bank. The protein minimization and protein preparation followed by the literature method [28, 29]. Detailed protein minimization procedure was given in supplementary information (available here). The highly active four compounds, 1c, 1e, 2c, and 2e, were sketched by the Marvin Sketch (version 5.3.0) tool, and 3D conformers were generated using the Ligand Prep module. The four compounds, 1c, 1e, 2c, and 2e, were docked with target proteins (i.e., DsbA (bacterial thiol disulfide oxidoreductase protein)) separately using the Glide module (Glide 4.0 version).

2.3. In Vitro Antibacterial Screening. The compounds 1a-1g and 2a-2g were evaluated for their antibacterial activity against the *Staphylococcus aureus* (ATCC-25923), *Klebsiella pneumoniae*, *Escherichia coli* (ATCC-25922), and *Pseudomonas aeruginosa* (ATCC-27853) based on previously reported techniques, and we used a bacterial strain [30, 31]. The minimum inhibitory concentration was also determined for all the synthesized compounds. DMSO (dimethylsulfoxide) at 64 g/mL was used as a solvent to dissolve the test samples separately. Twofold dilutions methods were used to prepare various dilutions (128, 64, 32, ..., 0.12 g/mL). 106 CFU of the suspension was inoculated onto wells and incubated for 24 hours at 36°C .

3. Results and Discussion

3.1. Characterization of ZnO NPs

3.1.1. Transmission Electron Microscopy (TEM). TEM examination was used to examine the morphology and particle size of ZnO NPs. Figure 5 depicts an overview of green produced ZnO NPs, which clearly demonstrates the NPs' spherical form and average size of 20 nm.

3.1.2. Scanning Electron Microscopy (SEM). SEM analysis indicated well-defined uniformly spherical ZnO NPs with particle aggregation. The extensively distributed charged surfaces of *Moringa oleifera* are excellent for binding metal ions from their aqueous precursor solution. Large lignin is found in *Moringa oleifera* leaves, seeds, flowers, pods, barks, and cellulose has a strong attraction for positively charged heavy metals. As a result, the *Moringa oleifera* had a negative charge. Figure 6 shows a SEM picture of ZnO NPs.

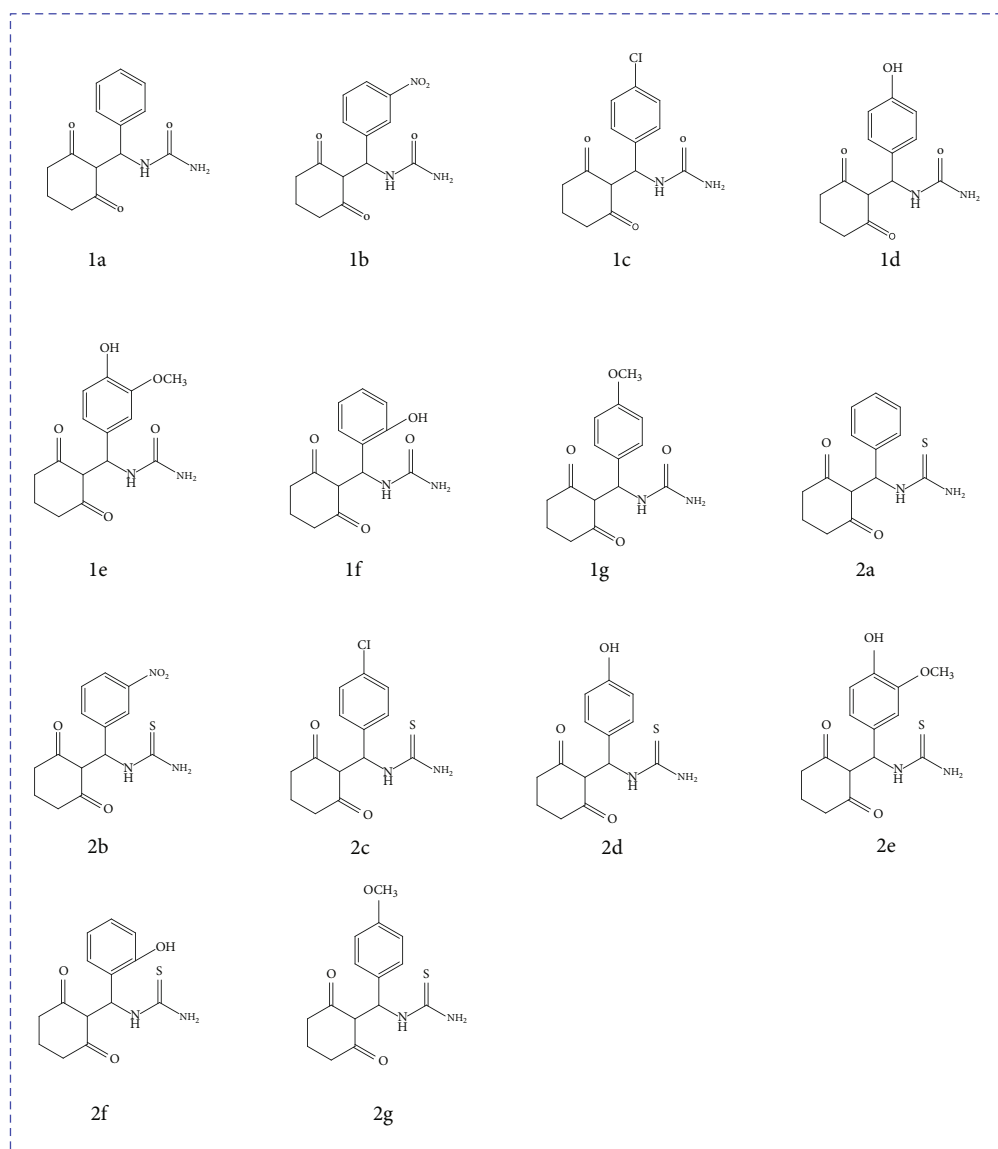


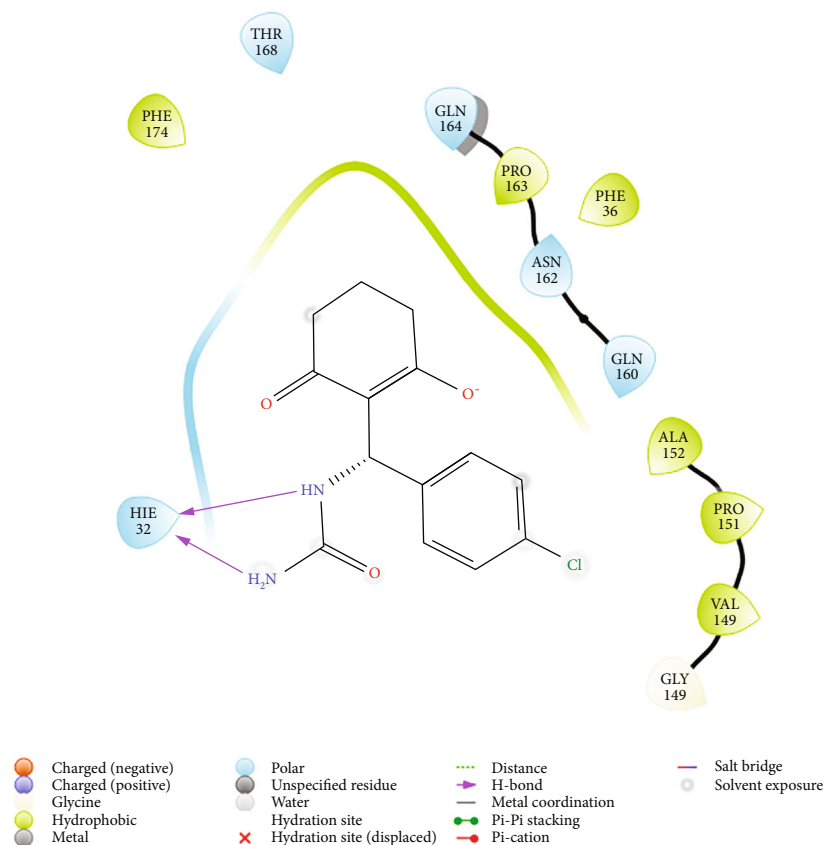
FIGURE 10: Structure of 1,3-cyclohexanedione moiety connected Mannich base derivatives.

TABLE 3: Docking results of synthesized compounds 1c and 2e with bacterial thiol disulfide oxidoreductase protein (PDB ID: 4WET).

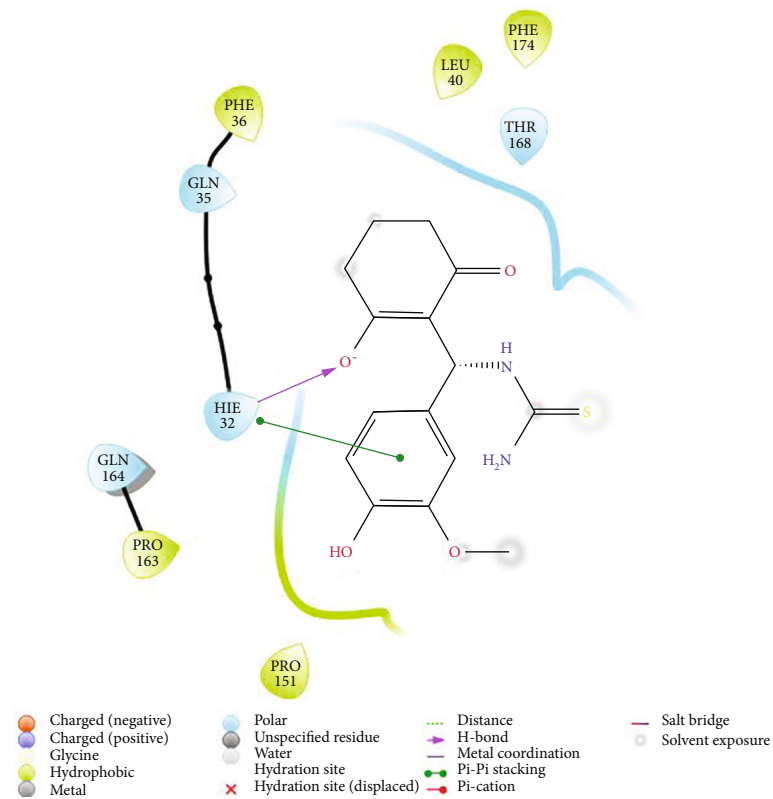
Name of the compounds	Docking score (kcal/Mol)	Glide energy (kcal/Mol)	Glide emodel (KJ/Mol)	Interacting residues	Bond length (Å)
1c	-4.3	-20.151	-51.915	His 32 (2) (H-bond)	2.08, 2.17
2e	-5.1	-20.942	-15.656	Pro 151 (2) (H-bond)	1.99, 2.30

3.1.3. Particle Size and Zeta Potential Analysis. Characterization of ZnO NPs by particle size analysis shows the size-dependent distribution of the nanoparticles (A); zeta potential analysis shows the surface charge of -56.80 mV for the ZnO NPs, which corresponds with the stability of the nanoparticles (B). In Figure 7(a), the dynamic light scattering (DLS) technique is used to measure the average polydispersity index (0.582) and particle size (201.6 nm) after a 200-fold aqueous

solution accompanied by heavy shaking to achieve 100–250 kilogram counts per second. Malvern Zetasizer Nano-ZS was used to measure the zeta potential of nanoparticles. The stability of the nanoparticles can be ascribed to their remarkably high zeta potential. The zeta potential is shown in Figure 7(b) as a distribution versus the total counts. This indicates that ZnO NPs are stable in an aqueous medium since the zeta potential value was -56.80 mV.



Compound-1c



Compound-2e

FIGURE 11: 2D interaction diagram between bacterial thiol disulfide oxidoreductase protein and synthesized compounds 1c and 2e.

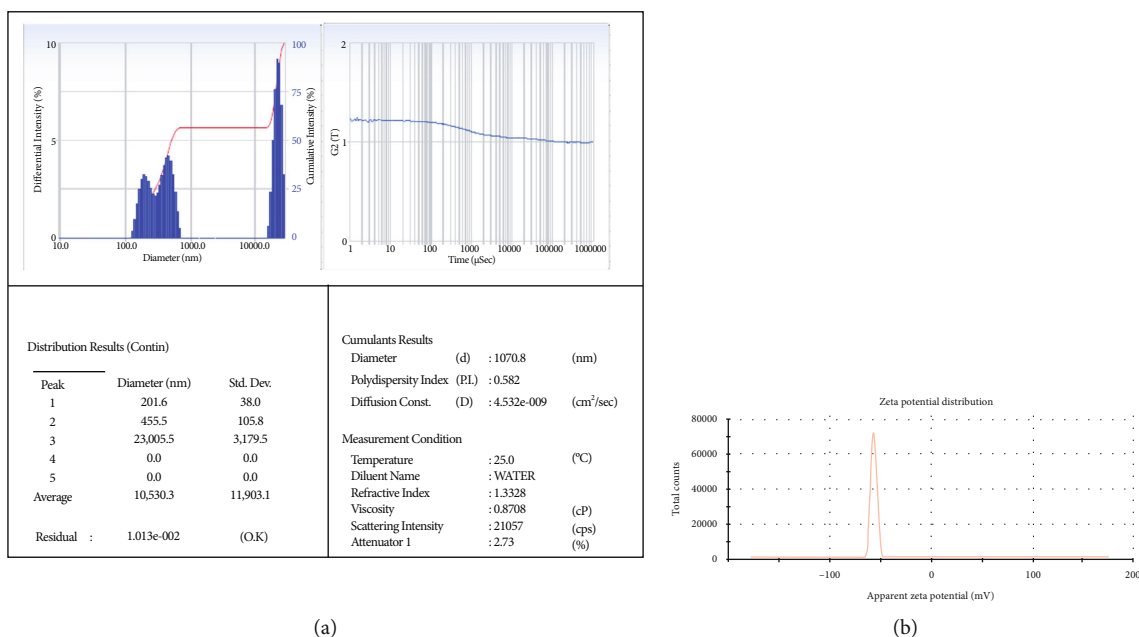


FIGURE 12: 3D interaction diagram between bacterial thiol disulfide oxidoreductase protein and synthesized compounds 1c (a) and 2e (d).

3.1.4. X-Ray Diffraction Analysis. XRD analysis was used to determine the structural and crystalline nature of the ZnO NPs. The four characteristic peaks detected in the XRD image at 2θ values ranging from 30 to 90 suggest that the biosynthesized zinc oxide nanostructure utilizing *Moringa oleifera* leaf extract was proven and confirmed [32]. 38.13° , 46.2° , 64.44° , and 77.36° correspond to the four powerful peaks shown in Figure 8.

3.1.5. Recovery of Catalyst. In the biosynthetic process, catalyst recovery is significant. Using the reaction of 1,3-cyclohexanedione derivatives (1a-1g) and (2a-2g) zinc oxide nanoparticle, we investigated their recyclability three times with nearly identical catalytic activity. After adding DMF, the ZnO NPs were separated by centrifugation and rinsed with EtOH to eliminate the remaining product. Figure 9 demonstrates the catalyst recyclability and recovery of the catalyst with a small loss of catalytic activity after at least 12-15 run times. By optimizing the reaction conditions, the application of the catalyst was examined. Table 1 shows the yield of a number of aldehydes used in the condensation reaction with the ZnO-NPs (1 mole percent) catalyst at room temperature in a reflux setting.

3.2. Chemistry

3.2.1. Synthetic Procedure of Compound (1a). All synthesized β -aminoketone derivatives (i.e., 1a-g and 2a-g) were characterized by FT-IR which showed various functional groups. From the FT-IR analysis, all the compounds displayed absorption bands at $3465\text{-}3420$, $3152\text{-}2908$, and $1752\text{-}1710\text{ cm}^{-1}$ corresponding to the NH_2 , CH-Ph, and C=O functional groups, respectively. In the proton NMR spectra of the compounds, 1a-1g and 2a-2g frequencies were observed at 5.74-

TABLE 4: Antibacterial activity of compounds 1a-1g and 2a-2g with MIC values.

Compound no.	Gram negative <i>E. coli</i>	<i>P. aeruginosa</i>	Gram positive <i>E. faecalis</i>	<i>S. aureus</i>
1a	142	132	98	16
1b	151	169	92	15
1c	141	165	63	16
1d	132	168	83	8
1e	143	138	96	32
1f	181	154	85	16
1g	228	161	82	16
2a	168	171	88	8
2b	188	288	92	4
2c	158	142	69	8
2d	154	188	82	16
2e	132	131	66	0.12
2f	126	141	98	15
2g	131	224	88	16
Mupirocin	128	>128	64	0.25

5.52, 5.54-4.35, and 4.38-4.21 corresponding to the NH_2 , CH-P, and CH in CHD protons. The ^{13}C NMR spectra exhibited peaks at 168.01-167.60, 204.02-203.82, and 189.21-182.01 corresponding to the C=O in urea, C=O in 1,3-cyclohexanedione, and C=S carbon, respectively. The results of the entire compounds and spectral data are given in supplementary Materials (available here). The substitutions of the synthesized

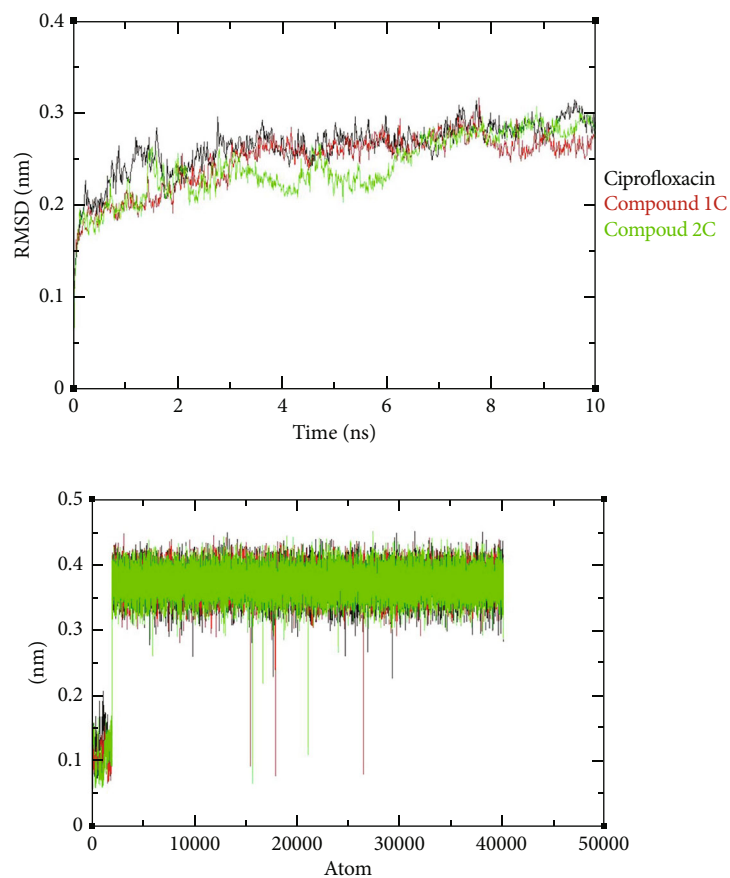


FIGURE 13: RMSD plot after ligand fit to the protein.

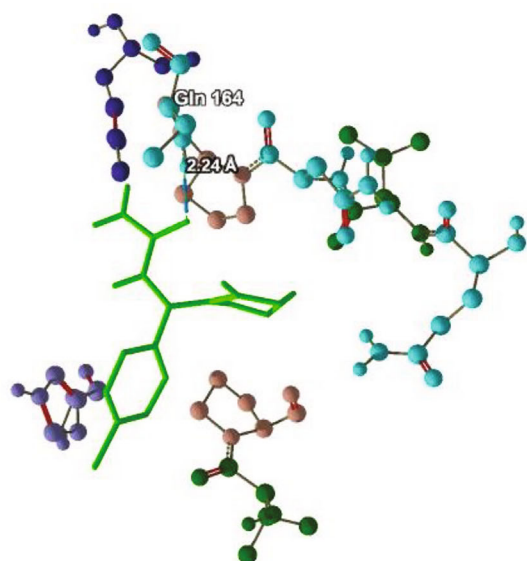
compounds 1a-g and 2a-g are given in Table 2. The synthesized of β -aminoketone derivative is shown in scheme 1. Structure of 1,3-cyclohexanedione moiety connected Mannich base derivatives is shown in Figure 10.

3.3. Molecular Docking Study for a Bacterial DsbA Protein. In this study, different interactions, including hydrogen bonds, π - π stacking, pi-cation, and hydrophobic and hydrophilic forces, were identified between the synthesized compounds and proteins (DsbA as a bacterial protein). The compounds 1c and 2e exhibited satisfactory docking scores with the bacterial protein. The detailed docking score, Glide energy, Glide module, and interaction residues are presented in Table 3. The 2D and 3D interaction diagrams are illustrated in (Figures 11 and 12). The compound 2e displayed significant inhibition ability with the binding energy (-5.1 kcal/mol) than compound 1c (binding energy: -4.3 kcal/mol), respectively. Compound 2e forms one hydrogen bond interaction with the target protein. The hydrogen atom from Hie32 amino acid residue and oxygen atom from $-C=O$ group of compounds 2e were involved in hydrogen bonding. The amino acid residue Hie 32 displayed π - π stacking interaction with aromatic ring of aldehyde scaffold from compound 2e. The amino acid residues of Phe36, Leu40, Pro151, Pro163, and Phe174 were involved in hydrophobic contacts. The residues of amino acids

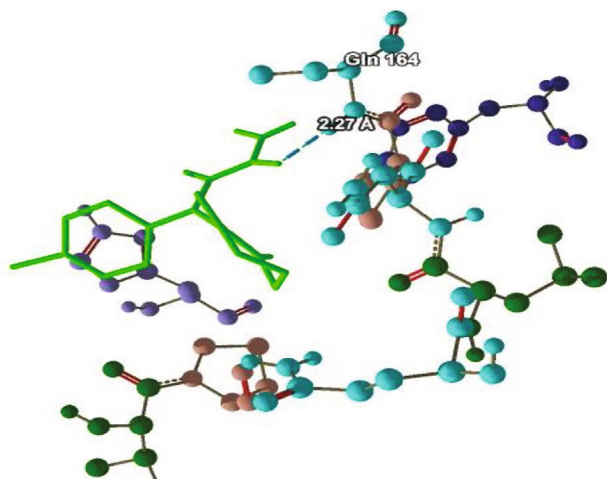
Hie32, Gln35, Gln164, and Thr168 were involved in polar contacts. Compound 1c forms two hydrogen bond interactions with the target protein. The oxygen atom from Hie32 amino acid residue and hydrogen atom from the $-NH_2$ and $-NH$ group of compound 1c was involved in hydrogen bonding. The amino acid residues of Phe36, Val150, Pro151, Ala152, Pro163 and Phe174 were involved in hydrophobic contacts. The residues of amino acids Hie32, Gln160, Asn162 and Gln164 were involved in polar contacts. It is possible to assume that the compounds achieved a reasonable docking score, based on the results along with essential interactions that could stabilize the compounds in the active site of a protein. From the above results, compound 2e exhibited the highest docking score of -5.1 (kcal/mol) compared to the other compounds.

3.4. In Vitro Antibacterial Activity Analysis. The urea derivatives of 1a-1g and 2a-2g were examination for their in vitro antibacterial activity against *E. coli*, *P. aeruginosa*, *E. faecalis*, and *S. aureus*. Mupirocin was used as a standard. Compound 1c ($63 \mu\text{g/mL}$, *E. faecalis*) and compound 2e ($0.12 \mu\text{g/mL}$, *S. aureus*) were highly active compared with the standard drug. MIC values are represented in Table 4.

3.5. Molecular Dynamic Simulation. The stability of protein-ligand complex structures of compounds 1c and 2c with DsbA



Compound 1c with 4WET protein



Compound 2c with 4WET protein

FIGURE 14: Molecular dynamic simulation of 1c and 2c with 4WET protein.

(4WET) was carried out by molecular dynamic (MD) simulation method using GROMACS. Root mean square deviation (RMSD) plot is an important to know the stability of the complex structure.

From the analysis of RMSD plot, the protein fluctuations after ligand fit into the protein were analyzed. All the 2 docked complex structures show that the complexes are stable because α backbone of protein was fluctuated within the 0.3 nm shown in Figure 13. Root mean square fluctuation (RMSF) is an important analysis to characterize the protein residues throughout the simulation time period. From the RMSF analysis, the protein residues were not fluctuated more, especially that the active residues Cys 30, His 32, Cys 33, Pro 151, and Gln 164 were within the range of 0.3 nm shown in Figure 14. During the period of simulation hydrogen bond interactions

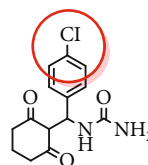
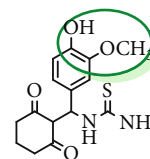
Compound 1c
Gram positive
(63 μ g/mL, *E. faecalis*)Compound 2e
Gram positive
(0.12 μ g/mL, *S. aureus*)

FIGURE 15: Comparison of highly active compounds 1c and 2e.

that was formed between the protein 4WET and drug and compounds, the compound 1c had interaction with the active site residue Gln 164 up to end of the period of simulation. The compound 2e had an interaction with Gln 164 at the 5th nano-second, and it is not continued afterwards. From this MD simulation analysis, the compound 1c is stable with the respective of protein, and it has good interaction with the active site residue of protein. Hence, this compound may suggest to good inhibitor against the 4WET protein.

Based on the result obtained from the molecular docking simulation, all of the two compounds had a good binding affinity. However, compound 2e (docking score: -5.1 kcal/mol), (Glide energy: -20.942 kcal/mol) attained the highest binding affinity when binding with the DsbA protein. From these results, it can be concluded that compounds 1c and 2e (docking score: -4.3 kcal/mol), (Glide energy: -20.151 kcal/mol), (docking score: -5.1 kcal/mol), and (Glide energy: -20.942 kcal/mol) effectively interacted through hydrogen bonding with the active site of above-mentioned protein, thereby contributing to their potential skin antibacterial inhibitory activity.

3.6. Structure-Activity Relationship. Comparison of highly active compounds 1a and 2e was shown in Figure 15. In light of the antibacterial after effects of urea with 1,3-cyclohexanedione and benzaldehyde, the fundamental SARs could be assessed and are shown in Figure 16. The NH_2 bunch present in the urea responded with the hydrogen holding space. In this way, urea might be expressed as an essential pharmacophoric requirement for antibacterial activity. The significances of the antibacterial activity (Table 2) revealed that most of the integrated compounds demonstrated differing degrees of restraint against tried microorganisms. Compounds 1c and 2e having chloro and -OH groups at a para position in phenyl moiety showed to be good active when compared with the standard mupirocin against (63 μ g/mL, *E. faecalis*) and 2e (0.12 μ g/mL, *S. aureus*). Compounds 1b and 2b, with electron-withdrawing nitro groups, displayed less antibacterial activity. The compounds 1a and 2a having no replacement for their aryl moiety displayed the least antibacterial activity. Moreover, the result of the docking studies revealed that potent compounds 1c (-4.3 kcal/mol) and 2e (-5.1 kcal/mol) show good binding affinity through hydrogen bonding.

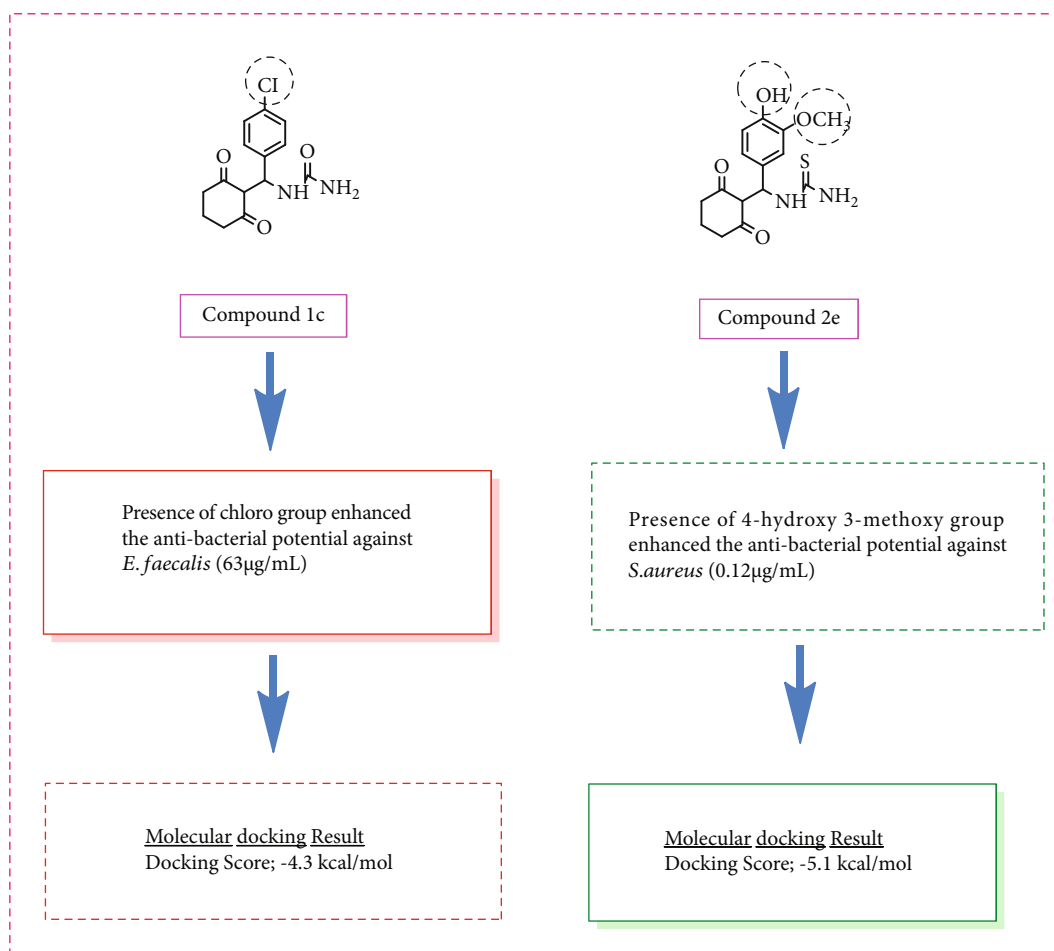


FIGURE 16: SAR relationship of highly active compounds.

4. Conclusions

Skin infections caused by bacteria have long been a clinical problem. As a result, we are concentrating on a green synthetic method for the synthesis of zinc oxide nanoparticles (ZnO NPs) utilizing *Moringa oleifera* extract, which can easily reduce zinc oxide ions into ZnO NPs. The antibacterial activity of the novel 1,3-cyclohexanedione compounds 1a-1g and 2a-2g was tested using ZnO NPs as a catalyst. When compared to the standard mupirocin, our antibacterial results showed that compound 1c (63 µg/mL, *E. faecalis*) and compound 2e (0.12 µg/mL, *S. aureus*) were extremely active against the two bacterial pathogens. Furthermore, the in silico analysis revealed that the two dynamic compounds 1c and 2e have high docking scores. As a result, the compounds 1c and 2e may be useful in the development of antibacterial agents. The application of this knowledge will result in the development of a green chemical approach to skin antibacterial research.

Data Availability

Our data are present along with our manuscript.

Conflicts of Interest

The authors declare no conflict of interest.

Acknowledgments

This work was funded by the Researchers Supporting Project number (RSP-2021/27), King Saud University, Riyadh, Saudi Arabia.

Supplementary Materials

The supplementary material used to support the findings of this study is included within the supplementary information files (the supplementary file contains ¹H-NMR and ¹³C-NMR spectra). (*Supplementary Materials*)

References

- [1] H. Sorg, D. J. Tilkorn, S. Hager, J. Hauser, and U. Mirastschijski, "Skin wound Healing: an update on the current knowledge and concepts," *European Surgical Research*, vol. 58, no. 1-2, pp. 81-94, 2017.
- [2] P. V. Baptista, M. P. McCusker, A. Carvalho, D. A. Ferreira, N. M. Mohan, and M. Martins, "Nano-strategies to fight

- multidrug resistant bacteria—"a battle of the titans";" *Frontiers in Microbiology*, vol. 9, p. 1441, 2018.
- [3] K. P. Miller, L. Wang, B. C. Benicewicz, and A. W. Decho, "Inorganic nanoparticles engineered to attack bacteria," *Chemical Society Reviews*, vol. 44, no. 21, pp. 7787–7807, 2015.
 - [4] N. X. Landén, D. Li, and M. Stähle, "Transition from inflammation to proliferation: a critical step during wound healing," *Cellular and Molecular Life Sciences*, vol. 73, no. 20, pp. 3861–3885, 2016.
 - [5] G. Yongwei, G. Qing, Y. Qing, Y. Meng, W. Shengzhang, and L. Jiyong, "Finite Element Analysis for Predicting Skin Pharmacokinetics of Nano Transdermal Drug Delivery System Based on the Multilayer Geometry Model," *International of nanomedicine*, vol. 15, pp. 6007–6018, 2020.
 - [6] N. Strbo, N. Yin, and O. Stojadinovic, "Innate and adaptive immune responses in wound epithelialization," *Advances in Wound Care*, vol. 3, no. 7, pp. 492–501, 2014.
 - [7] O. Takeuchi and S. Akira, "Pattern recognition receptors and inflammation," *Cell*, vol. 140, no. 6, pp. 805–820, 2010.
 - [8] M. Christopher, J. H. Thomas, L. Christine, J. Willis, and T. Simpson, "Resistance to and synthesis of the antibiotic mupirocin," *Microbiology*, vol. 8, no. 4, pp. 281–289, 2010.
 - [9] N. Bala, S. Saha, M. Chakraborty et al., "Green synthesis of zinc oxide nanoparticles using hibiscus subdariffa leaf extract: effect of temperature on synthesis, anti-bacterial activity and anti-diabetic activity," *RSC Advances*, vol. 5, no. 7, pp. 4993–5003, 2015.
 - [10] W. J. Rasmussen, E. Martinez, P. Louka, and G. D. Wingett, "Zinc oxide nanoparticles for selective destruction of tumor cells and potential for drug delivery applications," *Expert opinion on drug delivery*, vol. 7, no. 9, pp. 1063–1077, 2010.
 - [11] H. S. Yoon and J. D. Kim, "Fabrication and characterization of ZnO films for biological sensor application of FPW device," in *2006 15th IEEE International Symposium on the Applications of Ferroelectrics*, vol. 3, pp. 322–325, Sunset Beach, NC, USA, 2006.
 - [12] M. H. Xiong, "ZnO nanoparticles applied to bioimaging and drug delivery," *Advanced Materials*, vol. 25, no. 37, pp. 5329–5335, 2013.
 - [13] C. Dagdeviren, S. W. Hwang, Y. Su et al., "Transient, biocompatible electronics and energy harvesters based on ZnO," *Small*, vol. 9, pp. 3398–3404, 2013.
 - [14] L. Wang, Y. Kang, X. Liu, S. Zhang, W. Huang, and S. Wang, "ZnO nanorod gas sensor for ethanol detection," *Chem*, vol. 162, no. 1, pp. 237–243, 2012.
 - [15] S. E. Cross, B. Innes, M. S. Roberts, T. Tsuzuki, T. A. Robertson, and P. McCormick, "Human skin penetration of sunscreen nanoparticles: in-vitro assessment of a novel micronized zinc oxide formulation," *Skin Pharmacology and Physiology*, vol. 20, no. 3, pp. 148–154, 2007.
 - [16] J. Zhou, N. Xu, and Z. L. Wang, "Dissolving behavior and stability of ZnO wires in biofluids: a study on biodegradability and biocompatibility of ZnO nanostructures," *Advanced Materials*, vol. 18, no. 18, pp. 2432–2435, 2006.
 - [17] L. Nie, L. Gao, P. Feng, and J. Zhang, "Three-dimensional functionalized tetrapod-like ZnO Nanostructures for plasmid DNA delivery," *Small*, vol. 2, no. 5, pp. 621–625, 2006.
 - [18] G. Applerot, A. Lipovsky, R. Dror, and N. Perkas, "Enhanced antibacterial activity of nanocrystalline ZnO due to increased ROS-mediated cell injury," *Advanced Functional Materials*, vol. 19, no. 6, pp. 842–852, 2009.
 - [19] S. Nair, "Role of size scale of ZnO nanoparticles and microparticles on toxicity toward bacteria and osteoblast cancer cells," *Journal of Materials Science: Materials in Medicine*, vol. 20, no. S1, pp. 235–241, 2009.
 - [20] V. A. Kirthi, A. A. Rahuman, G. Rajakumar, and S. Marimuthu, "Acaricidal, pediculocidal and larvicidal activity of synthesized ZnO nanoparticles using wet chemical route against blood feeding parasites," *Parasitology research*, vol. 109, no. 2, pp. 461–472, 2011.
 - [21] A. Alkaladi, M. A. Abdelazim, and M. Afifi, "Antidiabetic activity of zinc oxide and silver nanoparticles on Streptozotocin-induced diabetic rats," *International Journal of Molecular Sciences*, vol. 15, no. 2, pp. 2015–2023, 2014.
 - [22] D. L. Lee, M. P. Prisbylla, T. H. Cromartie et al., "The discovery and structural requirements of inhibitors of 4-hydroxyphenylpyruvate dioxygenase," *Weed Science*, vol. 45, no. 5, pp. 601–609, 1997.
 - [23] F. Ndikuryayo, B. Moosavi, W. C. Yang, and G. F. Yang, "4-Hydroxyphenylpyruvate dioxygenase inhibitors: from chemical biology to agrochemicals," *Journal of Agricultural and Food Chemistry*, vol. 65, no. 39, pp. 8523–8537, 2017.
 - [24] E. A. Lock, M. K. Ellis, P. Gaskin et al., "From toxicological problem to therapeutic use: the discovery of the mode of action of 2-(2-nitro-4-trifluoromethylbenzoyl)-1,3-cyclohexanedione (NTBC), its toxicology and development as a drug," *Journal of Inherited Metabolic Disease*, vol. 21, no. 5, pp. 498–506, 1998.
 - [25] M. Arend, B. Westermann, and N. Risch, "Modern variants of the Mannich reaction," *Angewandte Chemie International Edition*, vol. 37, no. 8, pp. 1044–1070, 1998.
 - [26] M. G. Hall, M. F. Wilks, W. M. Provan, S. Eksborg, and B. Lumholtz, "Pharmacokinetics and pharmacodynamics of NTBC (2-(2-nitro-4-fluoromethylbenzoyl)-1,3-cyclohexanedione) and mesotrione, inhibitors of 4-hydroxyphenyl pyruvate dioxygenase (HPPD) following a single dose to healthy male volunteers," *British Journal of Clinical Pharmacology*, vol. 52, no. 2, pp. 169–177, 2001.
 - [27] D. Sharma, J. Rajputa, S. B. Kaitha, and M. Kaurb, "Synthesis of ZnO nanoparticles and study of their antibacterial and antifungal properties," *Thin Solid Films*, vol. 519, no. 3, pp. 1224–1229, 2010.
 - [28] R. Kalirajan, S. Vivekkulshrestha Sankar, and S. Jubie, "Docking studies, synthesis, characterization of some novel oxazine substituted 9-anilinoacridine derivatives and evaluation for their anti-oxidant and anticancer activities as topo isomerase II inhibitors," *European journal of medicinal chemistry*, vol. 56, pp. 217–224, 2012.
 - [29] L. A. Adams, P. Sharma, B. Mohanty et al., "Application of fragment-based screening to the design of inhibitors of Escherichia coli Dsb A," *Angewandte Chemie International Edition*, vol. 54, pp. 2179–2184, 2014.
 - [30] M. S. Khan, A. Husain, and S. Sharma, "New 4, 6-diacetyl resorcinol mannich bases: synthesis and biological evaluation," *Acta Poloniae Pharmaceutica*, vol. 67, no. 3, pp. 261–266, 2010.
 - [31] R. Sutherland, R. J. Boon, K. E. Griffin, P. J. Masters, B. Slocombe, and A. R. White, "Antibacterial activity of mupirocin (pseudomonic acid), a new antibiotic for topical use," *Antimicrobial agents and chemotherapy*, vol. 27, no. 4, pp. 495–498, 1985.
 - [32] C. Joel, M. Sheik, and M. Badhusha, "Green synthesis of ZnO nanoparticles using Phyllanthus emblica stem extract and their antibacterial activity," *Der Pharmacia Lettre*, vol. 8, pp. 218–223, 2016.